






Article

Effects of the full-scale substitution of strontium for calcium on the microstructure of brushite: $(\text{Ca}_x\text{Sr}_{1-x})\text{HPO}_4 \cdot n\text{H}_2\text{O}$ system

Mazen Alshaaer^{1,2*} , Ahmed S. Afify³ , Moustapha E. Moustapha⁴, Nagat Hamad^{1,5}, Gehan A. Hammouda⁴ and Fernando Rocha² 

¹Department of Physics, College of Science and Humanities in Al-Kharj, Prince Sattam bin Abdulaziz University, Al-Kharj 11942, Saudi Arabia; ²GeoBioTec Research Center, University of Aveiro, Campus de Santiago, 3810-193 Aveiro, Portugal; ³Department of Basic Sciences, Higher Institute of Engineering and Automotive and Energy, Technology, New Heliopolis, Cairo, Egypt; ⁴Department of Chemistry, College of Science and Humanities in Al-Kharj, Prince Sattam bin Abdulaziz University, Al-Kharj 11942, Saudi Arabia and ⁵Department of Physics and Mathematical Engineering, Faculty of Electronic Engineering, Monifia University, Shibin el Kom, Egypt

Abstract

Brushite ($\text{CaHPO}_4 \cdot 2\text{H}_2\text{O}$) is an important calcium phosphate encountered in bone tissue engineering and bone cement formulation. There are many studies on the synthesis and characterization of brushite, but full-scale substitution and replacement of Ca by Sr in brushite as a key element in medical and environmental applications has not yet been explored systematically. Therefore, this study aims to evaluate the effects of substitution of Ca by Sr on the microstructural and thermal properties of brushite, including the chemical phases present, crystallization, structural water and phase stability. The chemical phases were determined by means of powder X-ray diffraction. The thermal properties were studied by thermogravimetric analysis. Crystallization and surface morphology were analysed using scanning electron microscopy. Various properties were dependent on the incorporated Sr ions. The replacement percentage of Sr may be divided into two major stages: the first from 0% to 50%; and the second from 50% up to 100%. The $(\text{Ca}_x\text{Sr}_{1-x})\text{HPO}_4 \cdot n\text{H}_2\text{O}$ shows that micro-scale crystals of platy brushite formed in the first stage of Sr replacement, from 0% up to 50%. As Sr might inhibit the formation of crystals, crystal nucleation rates were reduced as the Sr percentage increased. An amorphous product formed as a result of 50% Sr replacement. The second stage of Sr replacement with Sr contents >50% yielded a new crystal morphology corresponding mainly to $\text{SrHPO}_4 \cdot n\text{H}_2\text{O}$. The complete replacement of Ca by Sr transforms the brushite with platy microcrystals into SrHPO_4 nanosheets.

Keywords: brushite, crystals, long-term stability, strontium hydrogen phosphate, thermogravimetric analysis

(Received 2 September 2020; revised 11 January 2021; Accepted Manuscript online: 4 February 2021; Associate Editor: Anne-Claire Gaillot)

Calcium phosphate (CaP) phases and minerals are used in a wide range of clinical, environmental and engineering applications. They are commonly used as substitutes in bones because their biochemical properties make them suitable for medical applications (Alshaaer *et al.*, 2017; Neves *et al.*, 2017; Radwan *et al.*, 2020) and they are chemically and structurally similar to the mineral phase of bone tissues. Different phases of CaPs serve as precursors in the preparation of biocements and bioceramics, showing potential in the field of advanced materials research and technology (Alshaaer *et al.*, 2013, 2017, 2020). In general, they show low toxicity, high bioactivity and good biocompatibility. In addition, they exhibit acceptable biodegradable rates and can bond directly to bones given their mineralogical structure and chemical composition resembling the mineral phases of teeth and natural bone (Alshaaer *et al.*, 2013, 2017; Khalifehzadeh & Arami, 2020). Therefore, CaPs are excellent candidates for bone tissue engineering, drug delivery and bone-related disease treatment (Shyong *et al.*, 2018; Khalifehzadeh &

Arami, 2020). In addition to their clinical and pharmaceutical applications, CaPs are used in fertilizers (Liu *et al.*, 2020) and as construction materials (Alshaaer *et al.*, 2011).

Brushite (dicalcium phosphate dehydrate; DCPD; $\text{CaHPO}_4 \cdot 2\text{H}_2\text{O}$) is one of the best known CaPs (Alkhraisat *et al.*, 2011; Alshaaer *et al.*, 2011). Brushite is formed by chemical reactions in slightly acidic solutions (Xue *et al.*, 2020). This mineral is stable in weakly acidic environments (pH 4.0–6.0) and at low temperatures (<80°C) (Kim *et al.*, 2015; Xue *et al.*, 2020). Therefore, it is usually metastable at neutral conditions (*i.e.* at pH ~7.4), indicating that it may be resorbed within relatively short periods, potentially causing fast substitution of bone material (Mert *et al.*, 2011; Luo *et al.*, 2018).

Large-scale ion replacements reportedly occur in a crystal if the two radii are the same and the valence of the substituted ion is equivalent (Alkhraisat *et al.*, 2011). Calcium and strontium meet these two conditions, and thus the two ions can replace each other in a crystal (Rokita *et al.*, 1993). The substitution of calcium by strontium in CaP phases such as hydroxylapatite (HA), amorphous CaP (ACP), octacalcium phosphate (OCP) and brushite has been investigated in the past (Sinusaite *et al.*, 2019; Amjad *et al.*, 2020; Wu *et al.*, 2020). Various bone cements loaded with Sr have been introduced (Tadier *et al.*, 2012; Schumacher & Gelinsky, 2015). The Ca substitution by Sr in

*Email: mazen.alshaaer@yahoo.com

Cite this article: Alshaaer M, Afify AS, Moustapha ME, Hamad N, Hammouda GA, Rocha F (2020). Effects of the full-scale substitution of strontium for calcium on the microstructure of brushite: $(\text{Ca}_x\text{Sr}_{1-x})\text{HPO}_4 \cdot n\text{H}_2\text{O}$ system. *Clay Minerals* 55, 366–374. <https://doi.org/10.1180/clm.2021.5>

Table 1. Composition of the $(\text{Ca}_x\text{Sr}_{1-x})\text{HPO}_4 \cdot n\text{H}_2\text{O}$ powders.

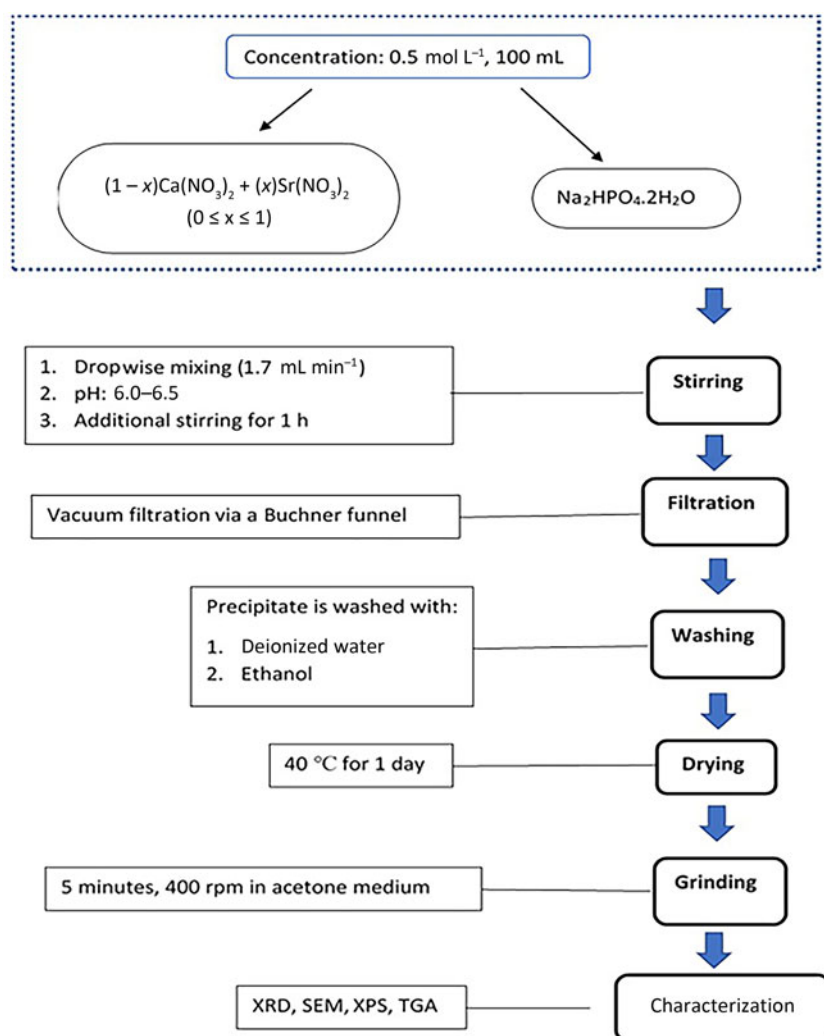
ID	Molar (M), pH = 6.5			Estimated chemical formula ($0 \leq n \leq 2$)
	Na_2HPO_4	$\text{Ca}(\text{NO}_3)_2$	$\text{Sr}(\text{NO}_3)_2$	
BSr0	1.0	1.0	0	$\text{CaHPO}_4 \cdot 2\text{H}_2\text{O}$
BSr2	1.0	0.8	0.2	$(\text{Ca}_{0.8}\text{Sr}_{0.2})\text{HPO}_4 \cdot 2\text{H}_2\text{O}$
BSr4	1.0	0.6	0.4	$(\text{Ca}_{0.6}\text{Sr}_{0.4})\text{HPO}_4 \cdot 2\text{H}_2\text{O}$
BSr5	1.0	0.5	0.5	$(\text{Ca}_{0.5}\text{Sr}_{0.5})\text{HPO}_4 \cdot n\text{H}_2\text{O}$
BSr6	1.0	0.4	0.6	$(\text{Ca}_{0.4}\text{Sr}_{0.6})\text{HPO}_4 \cdot n\text{H}_2\text{O}$
BSr10	1.0	0	1.0	SrHPO_4

CaPs is the most efficient (Alkhraisat *et al.*, 2011; Suguna & Sekar, 2011) because Ca sites in the brushite may be completely replaced by Sr, which is effective for bone-loss prevention. *In vitro* studies report that strontium ions (Sr^{2+}) may increase apoptosis and decrease the differentiation of osteoclasts. Meanwhile, Sr^{2+} ions improve cell growth and proliferation. Introducing Sr^{2+} decreases bone resorption and causes sustainable bone formation (Nielsen, 2004; Pina *et al.*, 2010; Sayahi *et al.*, 2020).

Brushite is one of the most important CaP minerals in bone tissue engineering. Its clinical applications include use as a bone-cement precursor (Roy *et al.*, 2012; Tamimi *et al.*, 2012). However, to date,

the potential of brushite as a bioactive material in the body has not received much attention. The partial or complete replacement of Ca in brushite with Sr to improve its performance as a biomaterial deserves further exploration. The present study therefore aims to synthesize and characterize pure brushite and to study the partial and complete replacement of Ca with Sr in brushite under fixed conditions in a so-called $(\text{Ca}_x\text{Sr}_{1-x})\text{HPO}_4 \cdot n\text{H}_2\text{O}$ system. The microstructure of the powders produced was investigated in terms of chemical phase, crystal morphology, thermal properties and shelf storage stability. The possibility of replacing Ca by Sr was explored here in view of the characteristics of the obtained compounds by means of complementary techniques: X-ray diffraction (XRD), scanning electron microscopy (SEM), thermogravimetric analysis (TGA) and ageing under ambient conditions.

Brushite is an important precursor of several bone cements and bioceramics (Alshaaer *et al.*, 2013, 2017). The novelty of this research lies in the study of the effects of the full-scale replacement of Ca by Sr as one of the most important elements in biomaterials (Kruppke *et al.*, 2020) starting from pure brushite. The ‘replacement’ in this study is defined as the substitution of Ca by Sr and maintaining the same conditions during the powder preparation. The crystal morphology, chemical composition and mineralogical structure are important factors in the preparation of the reactive components of bone

**Fig. 1.** Schematic diagram of the experimental design.

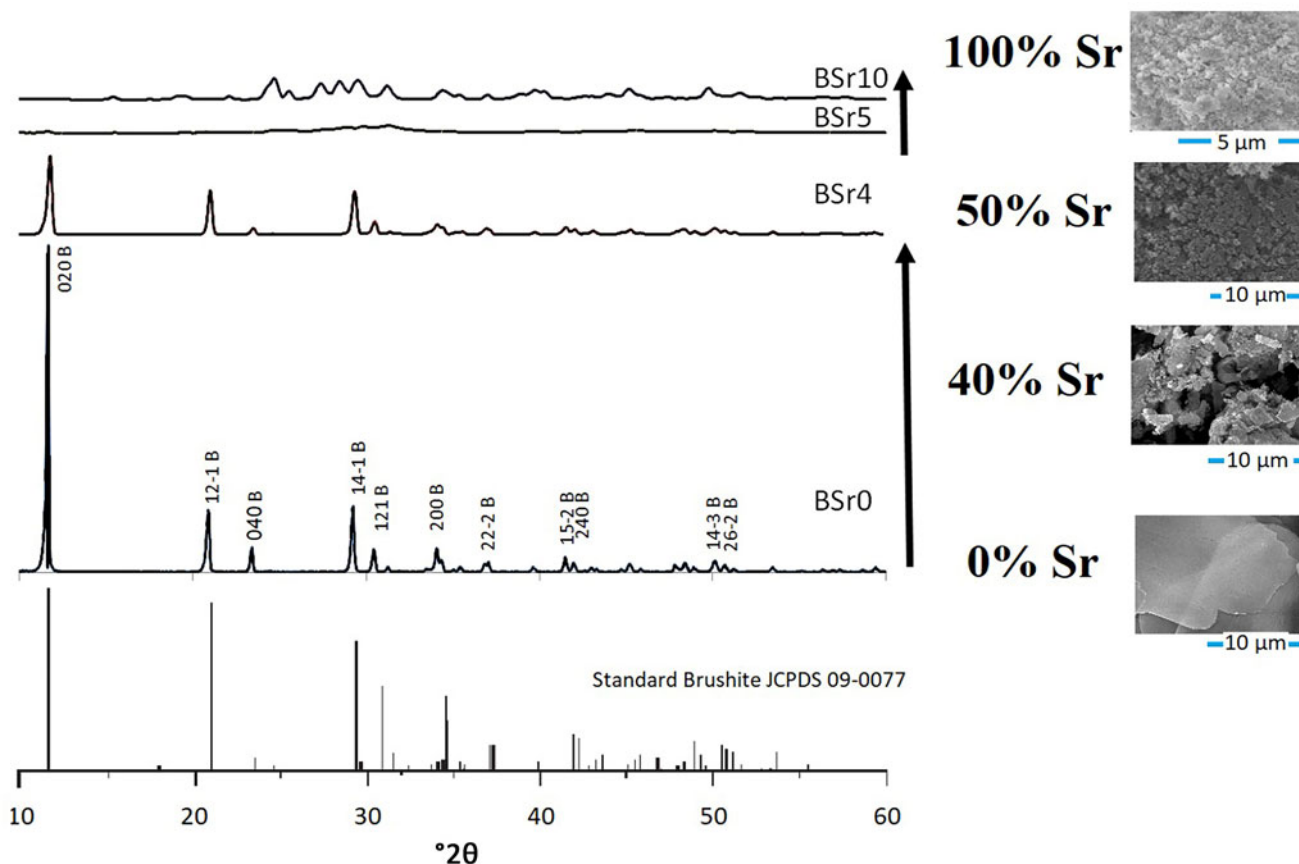


Fig. 2. XRD traces (left) and corresponding SEM images (right) of the $(\text{Ca}_x\text{Sr}_{1-x})\text{HPO}_4.n\text{H}_2\text{O}$ powders.

cements such as tetracalcium phosphates (Alshaaer *et al.*, 2013). Obviously, the high levels of replacement will result in new forms of crystals and probably other minerals. Accordingly, the scientific community should be able to select the appropriate range of replacements to synthesize a given biomaterial.

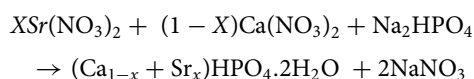
Experimental

Materials and chemicals

Sodium dihydrogen orthophosphate dihydrate ($\text{Na}_2\text{HPO}_4.2\text{H}_2\text{O}$) was purchased from Techno Pharmchem (India), while calcium nitrate tetrahydrate ($\text{Ca}(\text{NO}_3)_2.4\text{H}_2\text{O}$) and strontium nitrate ($\text{Sr}(\text{NO}_3)_2$) were supplied by LOBA Chemie (India). Distilled water ($0.055 \mu\text{S cm}^{-1}$) was acquired using a water purification system (PURELAB Option-Q, ELGA, UK). Each sample was weighed using a digital analytical balance (EX324N, OHAUS, USA) and stirring was performed on a magnetic stirrer (ISOTEMP, Fisher Scientific, China).

Synthesis of $(\text{Ca}_x\text{Sr}_{1-x})\text{HPO}_4.n\text{H}_2\text{O}$ powders

The synthesis of the $(\text{Ca}_x\text{Sr}_{1-x})\text{HPO}_4.n\text{H}_2\text{O}$ powders was performed at room temperature and is based on the following reaction:



Two starting solutions were prepared for the synthesis of various powders. The first solution was prepared by dissolving 0.05 mol of $\text{Na}_2\text{HPO}_4.2\text{H}_2\text{O}$ in 100 mL of deionized water, and the second solution resulted from dissolution of 0.05 mol of $\text{Ca}(\text{NO}_3)_2$ and/or $\text{Sr}(\text{NO}_3)_2$ in 100 mL of deionized water. The molar ratios of $\text{Ca}(\text{NO}_3)_2$ and $\text{Sr}(\text{NO}_3)_2$ were selected based on Table 1. The pH was fixed at 6.5 for all of the solutions. The powders were prepared according to Table 1.

Subsequently, 100 mL of the $\text{Ca}_x\text{Sr}_{1-x}(\text{NO}_3)_2$ ($0 \leq x \leq 1$) solution was added dropwise using a glass funnel with a glass stopcock (flow rate = 1.7 mL min^{-1}) to the $\text{Na}_2\text{HPO}_4.2\text{H}_2\text{O}$ solution under continuous stirring (450 rpm). This solution was stirred (200 rpm) at room temperature for 1 h to ensure a homogeneous mixture. The overall stirring period prior to filtering was ~2 h. The pH of the solution obtained was adjusted during stirring using an ammonia solution (25%; Labochemie, India) to form a white precipitate in a slightly acidic medium (pH 6.0–6.5) using a pH meter (Adwa, Romania). The precipitate was vacuum filtered using qualitative filter paper (45 μ , 12 cm; Double Rings, China) *via* a Buchner funnel, washed three times with deionized water and washed another three times with ethanol to reduce the possibility of agglomeration (Patil *et al.*, 2012; Piva *et al.*, 2015; Lu *et al.*, 2020), after which it was placed upon a watch glass and dried at 40°C overnight in a drying oven (ED53/E2; Binder, Germany).

After formation of the precipitate, an aliquot of the powder was washed with distilled water and dried using ethanol at 40°C. The remaining part was placed in open plastic containers without washing and air dried for 1 week. The powders were then

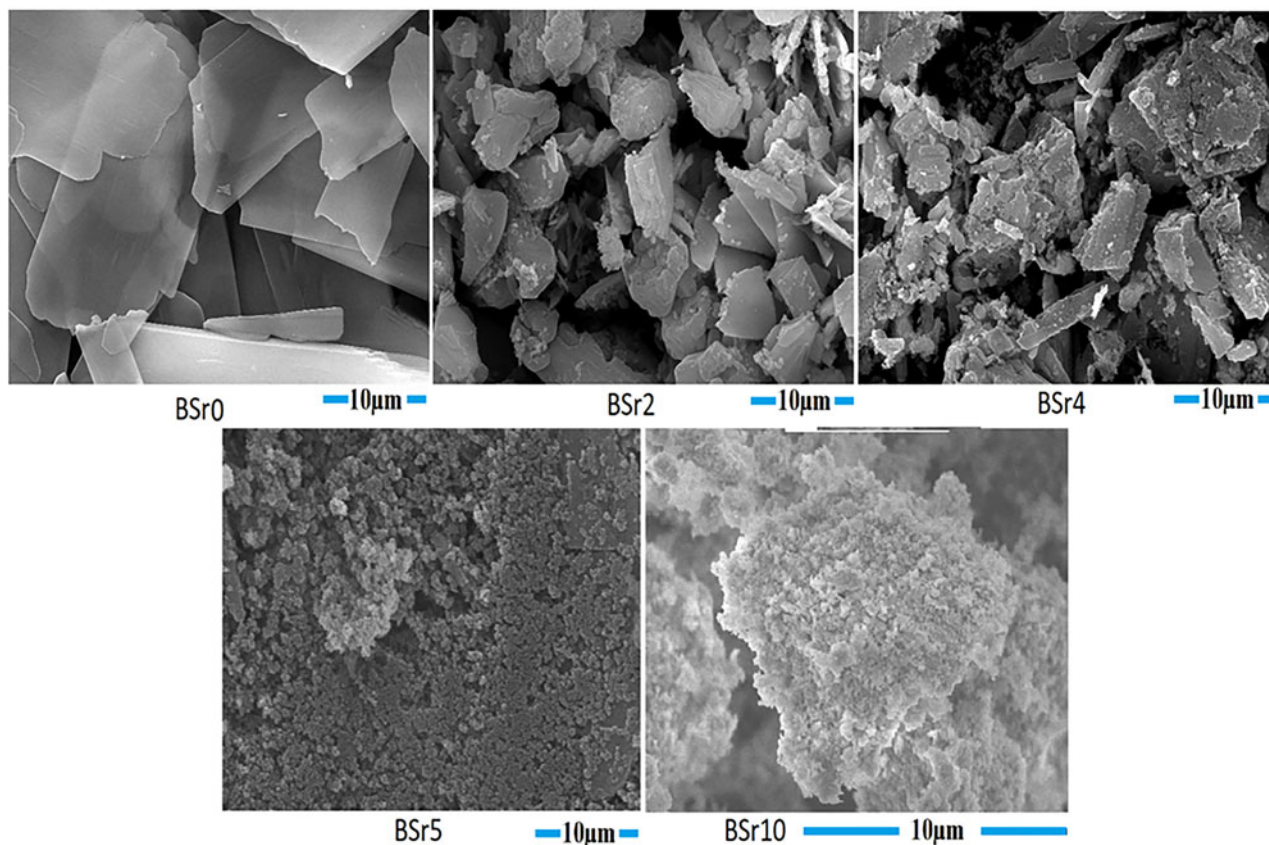


Fig. 3. SEM images of the $(\text{Ca}_x\text{Sr}_{1-x})\text{HPO}_4 \cdot n\text{H}_2\text{O}$ powders.

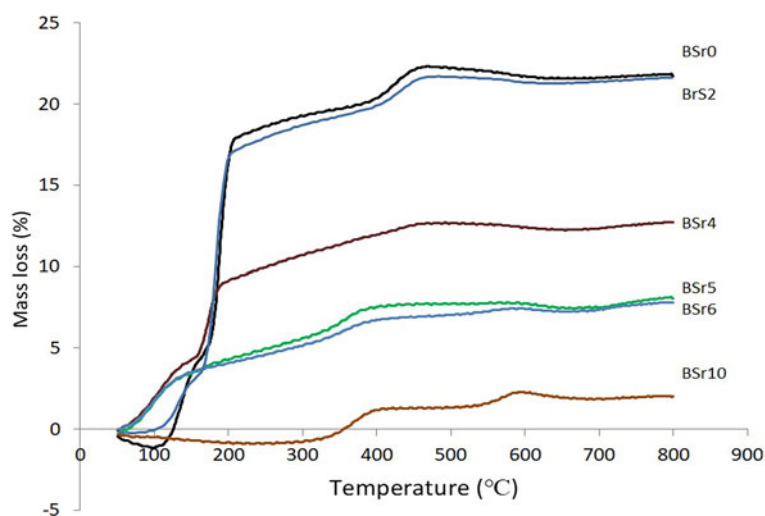


Fig. 4. Cumulative mass loss of the $(\text{Ca}_x\text{Sr}_{1-x})\text{HPO}_4 \cdot n\text{H}_2\text{O}$ powders with heating (TGA analysis).

disaggregated by grinding in a planetary mill for 15 min at a rotation rate of 7000 rpm, using zirconia grinding media and acetone as the disaggregation medium. After disaggregation, the powders were dried in air at room temperature for 2 h. Next, the dried powders were sieved to pass through a 200 μm sieve. The major steps of the experimental design are reported in Fig. 1.

Characterization

The amorphous and major crystalline phases of the powder samples were determined qualitatively using a Shimadzu XRD-6000

(Japan) with a cobalt tube, in a scanning range of $10\text{--}60^\circ 2\theta$ at a scan rate of 2°min^{-1} . A scanning electron microscope (Inspect F50; FEI, The Netherlands) was used to characterize the morphology of the specimens. The mass loss with heating of the powdered samples ($\sim 100 \text{ mg}$) was determined with a thermogravimetric analyser (TG 209 F1 Libra; Netzsch, Germany). The samples were heated in the $40\text{--}850^\circ\text{C}$ temperature range with a heating ramp of 5°C min^{-1} under a helium atmosphere. The surface chemistry and the elemental analysis of the powders obtained were characterized by means of X-ray photoelectron spectroscopy (XPS) with a Thermo K-Alpha XPS spectrometer (USA).

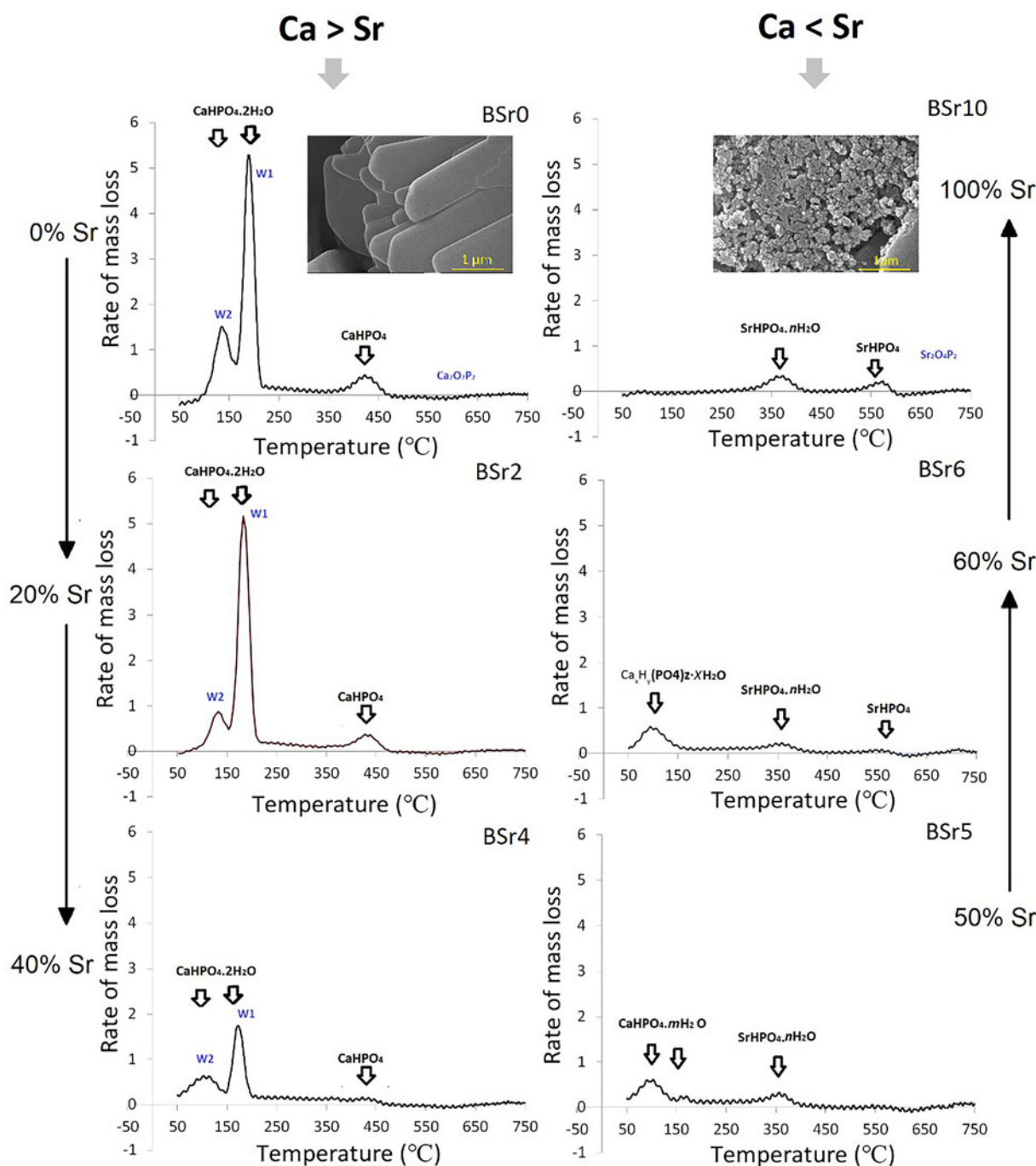


Fig. 5. Derivative of mass loss of the $(\text{Ca}_x\text{Sr}_{1-x})\text{HPO}_4.n\text{H}_2\text{O}$ powders as a function of temperature (DTG analysis).

Long-term stability at ambient conditions

The effect of ambient ageing on the microstructural stability of pure brushite (BSr0) and BSR2 (20% Sr) was studied. The samples were left at room temperature for 1, 2 and 20 months, and then were subjected to TGA analysis.

Results and discussion

The phase changes as a result of the full-scale replacement of Ca by Sr, from 0% to 100% in brushite, denoted here as the

$(\text{Ca}_x\text{Sr}_{1-x})\text{HPO}_4.n\text{H}_2\text{O}$ system, were analysed by XRD and SEM, as reported in Fig. 2. According to the XRD analysis, there are two different phases corresponding to different degrees of Sr replacement. The first phase includes 0–50% replacement of Sr phases (BSr0–BSr5), while in the second phase Sr replacement was from 50 to 100% (BSr5–BSr10).

The first phase ($\text{Sr}/\text{Ca} < 1$)

The XRD trace corresponding to the brushite powder BSR0 confirmed that the sample is crystalline and is composed of pure

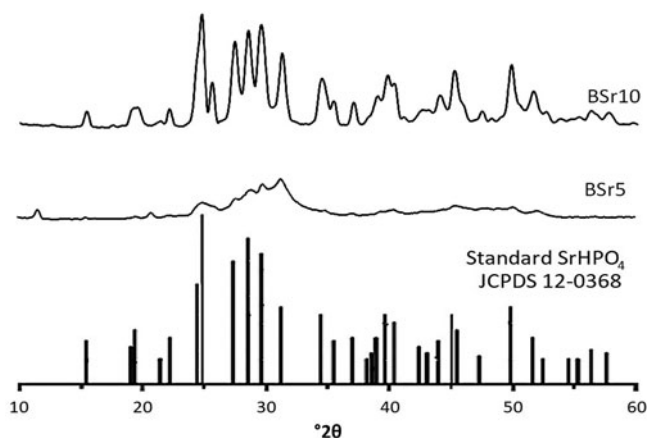


Fig. 6. XRD traces of the second stage of Sr replacement from 50% (BSr5) to 100% (BSr10).

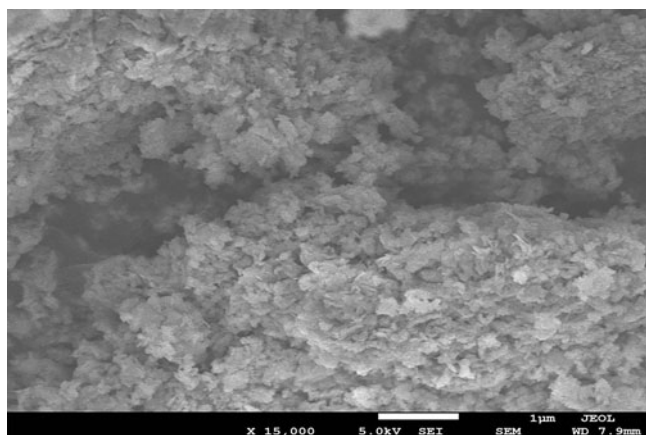


Fig. 7. SEM image of SrHPO₄ nanosheets (BSr10).

brushite with a monoclinic structure. The BSr0 brushite crystals were grown in proportion to the three major planes, namely (020), (121) and (141). The high-intensity XRD peak at 11.68°2θ intensity (Fig. 2) indicates that the crystal growth is mainly along the (020) crystallographic plane (Rokita *et al.*, 1993). The BSr0 brushite powder consisted of large, platy crystals, as observed by SEM (Fig. 3) (Suguna & Sekar, 2011). These platy crystals were very thin (~200 nm), but their width and elongation were ~10 µm and 20 µm, respectively (Tadier *et al.*, 2012). The platy morphology is typical of precipitated brushite (Schmacher & Gelinsky, 2015; Kruppke *et al.*, 2020).

Brushite is classified as a water-bearing phosphate (Sayahi *et al.*, 2020); heating BSr0 at a temperature of 800°C leads to the loss of ~22% of its mass (Fig. 4). Consequently, a portion of its chemically bound water is released during transformation (Liu *et al.*, 2020), while the remainder of the bound molecules re-phase themselves to form new CaP phases under alkaline conditions (Shyong *et al.*, 2018). Replacement by Sr of up to 20% (BSr2) did not lead to a significant change in the mass loss. However, the mass loss decreased significantly (by ~38%) after Sr replacement increased to 40% (BSr4). The decrease in structural water continued with increasing Sr contents, while the main features of the brushite mineral disappeared (Fig. 1).

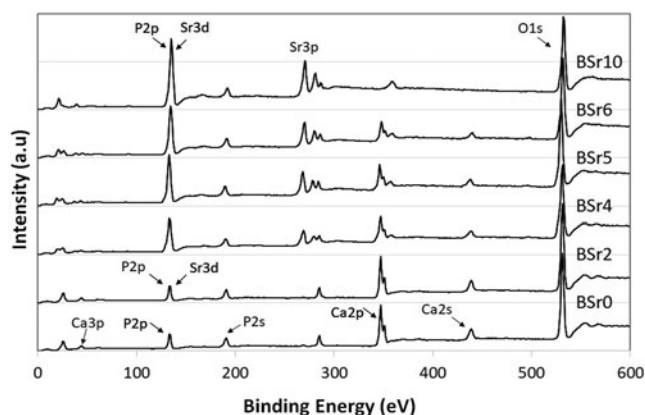


Fig. 8. XPS spectra of the (Ca_xSr_{1-x})HPO₄.nH₂O powders.

Brushite features water molecules with hydrogen bonds in its lattice and adsorbed water molecules on its surface (Tortet *et al.*, 1997; Gashti *et al.*, 2016). These water molecules are released in the 80–220°C temperature range, as is indicated by the extensive mass loss (Fig. 5). The crystal structure of brushite contains compact sheets consisting of parallel chains in which Ca ions are coordinated by six P atoms and two O atoms belonging to the water molecules (Alshaaer *et al.*, 2011). In addition to the adsorbed water molecules on its surface, two slightly different types of water molecules exist in brushite; one (W1) is linked to the phosphate oxygen by strong hydrogen bonds, whereas the other (W2) presents longer and weaker hydrogen bonds (BSr0; Fig. 5) (Tortet *et al.*, 1997; Suguna & Sekar, 2011). The corresponding dehydration peaks of the two water molecules (W1 and W2) are observed in BSr0, BSr2 and BSr4 (Fig. 5). These features of the brushite crystals, with the characteristic presence of two water molecules, disappear with an increase in the Sr replacement to >50% (*i.e.* in samples BSr5, BSr6 and BSr10; Fig. 5). The removal of the two structural water molecules at 220°C results in the transformation of brushite into monetite (CaHPO₄). Monetite decomposes at ~400°C to form calcium pyrophosphate (Ca₂O₇P₂).

The second phase (Sr/Ca >1)

In the second replacement phase, after replacement of Ca by Sr at >50% (samples BSr5–BSr10), all of the XRD peaks corresponding to brushite diminished (Fig. 2). Moreover, a semi-amorphous phase formed with 50% Sr replacement (BSr5; Fig. 6). The XRD trace of BSr10 (Fig. 6) is consistent with the standard data of β-type SrHPO₄ (JCPDS Card No. 12-0368), indicating that the obtained sample had a purely hexagonal crystal structure (Zhuang *et al.*, 2015). The SEM images show that sample BSr10 is composed of nanosheets (Fig. 7). Although the method of preparing the powders is different, there is a noteworthy matching of the results with those from previous studies, particularly the XRD traces (Zhuang *et al.*, 2015).

Figure 5 shows the formation of structural water corresponding to SrHPO₄ in the second stage of Sr replacement, from 50% to 100%. Three zones of decomposition of (Ca_xSr_{1-x})HPO₄.nH₂O for all of the samples are observed with Sr replacement of ~50% (BSr5). In the first zone, the weight loss results from the removal of surface-adsorbed water molecules and brushite-like crystals. This zone disappeared at 100% Sr replacement (BSr10) with the formation of pure SrHPO₄. A significant weight loss for crystals with Sr

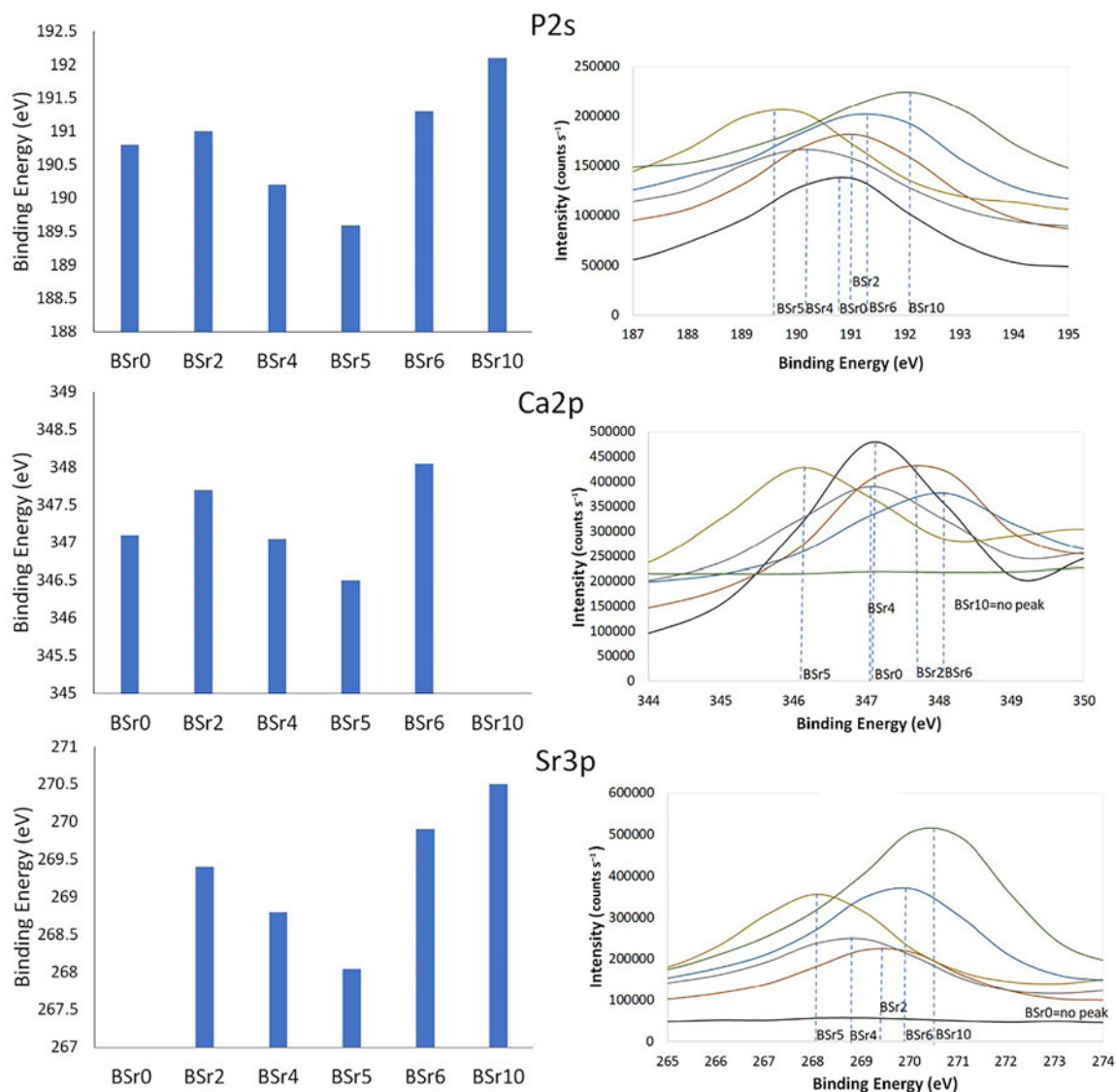


Fig. 9. XPS analysis of the chemical states of the elements (P2s, Ca2p, and Sr3p) in the $(\text{Ca}_x\text{Sr}_{1-x})\text{HPO}_4.n\text{H}_2\text{O}$ powders.

replacement >40% (BSr5, BSr6 and BSr10) occurred at the second zone between 320°C and 400°C due to the generation of Sr–O–P₂O₅ (Roming & Feldmann, 2008). The degradation of crystals began at 540°C and continued up to 600°C. This decomposition led to the transformation of SrHPO₄ into Sr₂O₄P₂.

Elemental and chemical composition

The XPS analysis was used to evaluate the influence of the Sr content on the surface chemistry and chemical state of the elements P, Ca and Sr in the $(\text{Ca}_x\text{Sr}_{1-x})\text{HPO}_4.n\text{H}_2\text{O}$ powders (Fig. 8). Additional peaks of Sr3p and Sr3d were clearly detectable in the powders with Sr contents (BSr2, BSr4, BSr5, BSr6 and BSr10). With increasing Sr content, from BSr0 up to BSr10, the peak intensities of Sr3d and Sr3p increased gradually and the peaks of Ca2s and Ca2p decreased gradually. No change was detected in the peaks of P2s. The envelopes of the P2p and Sr3d peaks at ~133.6 eV overlapped because of the proximity of the Sr3d and P2p (132–133 eV) lines (He *et al.*, 2016).

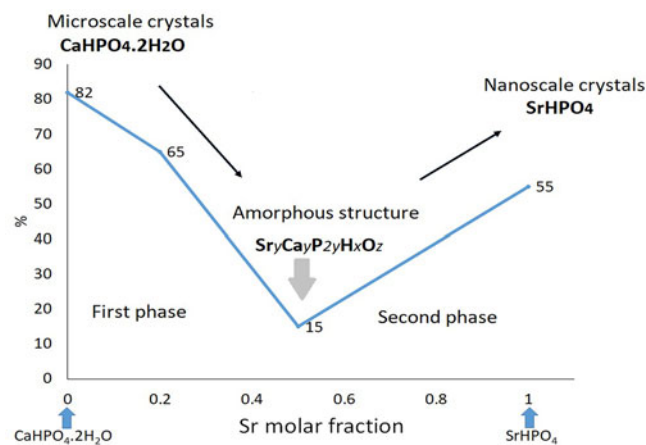


Fig. 10. Qualitative degree of crystal order of the $(\text{Ca}_x\text{Sr}_{1-x})\text{HPO}_4.n\text{H}_2\text{O}$ mineral system as a function of Sr molar fraction (analysis carried out on XRD traces using the Match! software package).

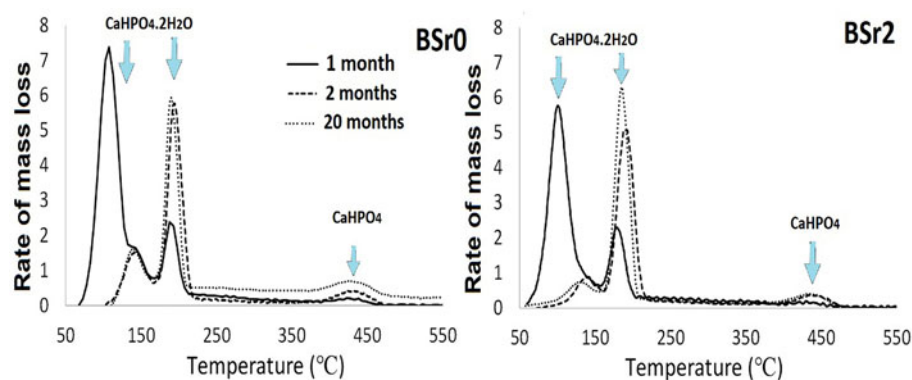


Fig. 11. Effect of ambient ageing on the thermal properties of brushite.

These results confirm that the peak intensities of P, Ca and Sr are comparable to the powder compositions reported in Table 1.

The XPS analysis of the chemical state of the elements (P2s, Ca2p and Sr3p) in the $(\text{Ca}_x\text{Sr}_{1-x})\text{HPO}_4 \cdot n\text{H}_2\text{O}$ powders is shown in Fig. 9. The binding energies of P2s, Ca2p and Sr3p exhibit the same trends with increasing Sr content. Replacement of Ca by 20% Sr (sample BSR2) resulted in a slight increase in the binding energies of P2s and Ca2p, from 190.8 to 191.0 eV and from 347.1 eV to 347.7 eV, respectively (Fig. 9). Increasing the Sr content to 40% and 50% (samples BSR4 and BSR5) resulted in decreasing the binding energies of P2, Ca2p and Sr3p. Further increasing the Sr content (samples BSR6 and BSR10) caused an observable increment in the binding energies of the three elements P2, Ca2p and Sr3p. BSR5 represents the inflection point in this ion exchange, which is in good agreement with the XRD and TGA results (Figs 2 & 5).

The XPS results confirmed that Sr was incorporated into the $(\text{Ca}_x\text{Sr}_{1-x})\text{HPO}_4 \cdot n\text{H}_2\text{O}$ lattice. The incorporation of Sr modified the crystal environment of the Ca2p ions, leading to an initial increase in the Ca binding energy. The minimum binding energies of P2s, Ca2p and Sr3p were recorded at the 50% replacement of Ca by Sr. This indicates that the lattice structure was distorted and a semi-amorphous phase was formed (Fig. 2). The lattice was rearranged again when increasing the Sr replacement above the level of 50% and strong chemical binding energies developed, which is in good agreement with the XRD results (Fig. 2).

Mechanism behind the full-scale Sr replacement

The crystal order of the $(\text{Ca}_x\text{Sr}_{1-x})\text{HPO}_4 \cdot n\text{H}_2\text{O}$ system as a function of the Sr molar fraction (analysis carried out on XRD traces using *Match!* software) is reported in Fig. 10. The crystal order appears to coincide with the previous results (cf. Figs 2 & 3), as increasing the replacement of Sr up to 50% would lead to the formation of a semi-crystalline phase (Fig. 9), yielding a decreased degree of crystal order from 82% to just 15% (Alkhraisat *et al.*, 2011). Increasing the replacement of Ca by Sr to >50% produced crystals of a new compound, which form SrHPO_4 nanosheets after the Ca is fully substituted by Sr (Romig & Feldmann, 2008; Zhuang *et al.*, 2015). The degree of crystal order increased from 15% up to 55% by increasing the replacement of Ca by Sr from 50% to 100%. The binding energies of Ca, Sr and P (Fig. 9) show trends that are similar to the crystal order.

Long-term stability at ambient conditions

The series BSR0 and BSR2 exhibit the same thermal behaviour after ambient ageing (Fig. 11). The greatest changes in thermal properties and structural water occur during the first 2 months of ageing. In contrast, the structural water of brushite corresponding to the stronger bond (W1) at 210°C increased significantly during this period of ageing (2 months), while the abundance of monetite, with its dehydration peak at 370–470°C, increased significantly for both samples. Increasing the ambient ageing to 20 months barely changed the structural water content. These results confirm that the first 2 months of ageing are most important for the full crystallization of brushite and the formation of stable microstructures.

Conclusions

In this work, we investigated the full-scale substitution and replacement of Ca by Sr in the microstructure of the $(\text{Ca}_x\text{Sr}_{1-x})\text{HPO}_4 \cdot n\text{H}_2\text{O}$ system using various analytical techniques. The results obtained show clearly that there are two stages of Sr replacement. In the first stage, from 0% up to 50%, the brushite crystals retain their features.

Replacement of Ca with 50% Sr results in the formation of a semi-amorphous phase. The second stage of Sr replacement (from 50% up to 100%) transformed the brushite into a new crystalline system based on Sr. This is due to the fact that as the Ca content decreases in the system, supersaturation with respect to brushite decreases while it increases with respect to SrHPO_4 . Finally, full replacement of Ca by Sr in the $(\text{Ca}_x\text{Sr}_{1-x})\text{HPO}_4 \cdot n\text{H}_2\text{O}$ system transforms the brushite crystals into SrHPO_4 nanosheets.

The most substantial changes in thermal properties and structural water occur in the first 2 months of ageing, when the structural water of brushite corresponding to the stronger bond (W1) at 210°C increased. These results also confirm that the first 2 months of brushite ageing are vital for the completion of crystallization and to obtain a stable microstructure.

References

- Alkhraisat M.H., Rueda C. & Cabarcos E.L. (2011) Strontium ions substitution in brushite crystals: the role of strontium chloride. *Journal of Functional Biomaterials*, 2, 31–38.
- Alshaer M., Abdel-Fattah E., Saadeddin I., Al Battah F., Issa K.I. & Saffarini G. (2020) The effect of natural fibres template on the chemical and

- structural properties of biphasic calcium phosphate scaffold. *Materials Research Express*, **7**, 065405.
- Alshaaer M., Cuypers H., Mosselmans G., Rahier H. & Wastiels J. (2011) Evaluation of a low temperature hardening inorganic phosphate cement for high-temperature applications. *Cement and Concrete Research*, **41**, 38–45.
- Alshaaer M., Cuypers H., Rahier H. & Wastiels J. (2011) Production of monetite-based inorganic phosphate cement (M-IPC) using hydrothermal post curing (HTPC). *Cement and Concrete Research*, **41**, 30–37.
- Alshaaer M., Kailani M.H., Ababneh N., Mallouh S.A.A., Sweileh B. & Awidi A. (2017) Fabrication of porous bioceramics for bone tissue applications using luffa cylindrical fibres (LCF) as template. *Processing and Application of Ceramics*, **11**, 13–20.
- Alshaaer M., Kailani M.H., Jafar H., Ababneh N. & Awidi A. (2013) Physicochemical and microstructural characterization of injectable load-bearing calcium phosphate scaffold. *Advances in Materials Science and Engineering*, **2013**, 149261.
- Amjad R.J., Sattar A. & Dousti M.R. (2020) Upconversion and 1.53 μm near-infrared luminescence study of the Er^{3+} - Yb^{3+} co-doped novel phosphate glasses. *Optik*, **200**, 163426.
- Gashti M.P., Stir M. & Jurg H. (2016) Growth of strontium hydrogen phosphate/gelatin composites: a biomimetic approach. *New Journal of Chemistry*, **40**, 5495–5500.
- He L., Dong G. & Deng C. (2016) Effects of strontium substitution on the phase transformation and crystal structure of calcium phosphate derived by chemical precipitation. *Ceramics International*, **42**, 11918–11923.
- Khalifehzadeh R. & Arami H. (2020) Biodegradable calcium phosphate nanoparticles for cancer therapy. *Advances in Colloid and Interface Science*, **279**, 102157.
- Kim Y., Lee S.Y., Roh Y., Lee J., Kim J., Lee Y. et al. (2015) Optimizing calcium phosphates by the control of pH and temperature via wet precipitation. *Journal of Nanoscience and Nanotechnology*, **15**, 10008–10016.
- Kruppke B., Heinemann C., Gebert A., Rohnke M., Weiß M., Henß A. et al. (2020) Strontium substitution of gelatin modified calcium hydrogen phosphates as porous hard tissue substitutes. *Journal of Biomedical Materials Research Part A*, doi: 10.1002/jbm.a.37057.
- Liu Y., Ma R., Li D., Qi C., Han L., Chen M. et al. (2020) Effects of calcium magnesium phosphate fertilizer, biochar and spent mushroom substrate on compost maturity and gaseous emissions during pig manure composting. *Journal of Environmental Management*, **267**, 110649.
- Lu B.-Q., Willhammar T., Sun B.-B., Hedin N., Gale J. D. & Gebauer D. (2020) Introducing the crystalline phase of dicalcium phosphate monohydrate. *Nature Communications*, **11**, 1546.
- Luo J., Engqvist H. & Persson C. (2018) A ready-to-use acidic, brushite-forming calcium phosphate cement. *Acta Biomaterialia*, **81**, 304–314.
- Mert I., Mandel S. & Tas A.C. (2011) Do cell culture solutions transform brushite ($\text{CaHPO}_4 \cdot 2\text{H}_2\text{O}$) to octacalcium phosphate ($\text{Ca}_8(\text{HPO}_4)_2(\text{PO}_4)_4 \cdot 5\text{H}_2\text{O}$)? Pp. 79–94 in: *Advances in Bioceramics and Porous Ceramics IV* (R. Narayan & P. Colombo, editors). John Wiley & Sons, Hoboken, NJ, USA.
- Neves N., Linhares D., Costa G., Ribeiro C.C. & Barbosa M.A. (2017) *In vivo* and clinical application of strontium-enriched biomaterials for bone regeneration: a systematic review. *Bone & Joint Research*, **6**, 366–375.
- Nielsen S.P. (2004) The biological role of strontium. *Bone*, **35**, 583–588.
- Patil S.B., Jena A. & Bhargava P. (2012) Influence of ethanol amount during washing on deagglomeration of co-precipitated calcined nanocrystalline 3YSZ powders. *International Journal of Applied Ceramic Technology*, **10**, E247–E257.
- Pina S., Torres P.M., Goetz-Neunhoffer F., Neubauer J. & Ferreira J.M.F. (2010) Newly developed Sr-substituted α -TCP bone cements. *Acta Biomaterialia*, **6**, 928–935.
- Piva R.H., Piva D.H., Pierri J., Montedo O.R.K. & Morelli M.R. (2015) Azeotropic distillation, ethanol washing, and freeze drying on coprecipitated gels for production of high surface area 3Y-TZP and 8YSZ powders: a comparative study. *Ceramics International*, **41**, 14148–14156.
- Radwan N.H., Nasr M., Ishak R.A., Abdeltawa N.F. & Awad G.A. (2020) Chitosan-calcium phosphate composite scaffolds for control of post-operative osteomyelitis: fabrication, characterization, and *in vitro*-*in vivo* evaluation. *Carbohydrate Polymers*, **244**, 116482.
- Rokita E., Hermes C., Nolting H. & Ryzek J. (1993) Substitution of calcium by strontium within selected calcium phosphates. *Journal of Crystal Growth*, **130**, 543–552.
- Roming M. & Feldmann C. (2008) Selective synthesis of α - and β - SrHPO_4 nanoparticles. *Journal of Materials Science*, **43**, 5504.
- Roy M., DeVoe K., Bandyopadhyay A. & Bose S. (2012) Mechanical property and *in vitro* biocompatibility of brushite cement modified by polyethylene glycol. *Materials Science and Engineering C*, **32**, 2145–2152.
- Sayahi M., Santos J., El-Feki H., Charvillat C., Bosc F., Karacan I. et al. (2020) Brushite (Ca_xM) $\text{HPO}_4 \cdot 2\text{H}_2\text{O}$ doping with bioactive ions ($\text{M} = \text{Mg}^{2+}$, Sr^{2+} , Zn^{2+} , Cu^{2+} , and Ag^+): a new path to functional biomaterials? *Materials Today Chemistry*, **16**, 100230.
- Schumacher M. & Gelinsky M. (2015) Strontium modified calcium phosphate cements – approaches towards targeted stimulation of bone turnover. *Journal of Materials Chemistry B*, **3**, 4626–4640.
- Shyong Y.-J., Chang K.-C. & Lin F.-H. (2018) Calcium phosphate particles stimulate exosome secretion from phagocytes for the enhancement of drug delivery. *Colloids and Surfaces B: Biointerfaces*, **1711**, 391–397.
- Sinusaitė L., Renner A.M., Schütz M.B., Antuzevics A., Rogulic U., Grigoraviciute-Puroniene I. et al. (2019) Effect of Mn doping on the low-temperature synthesis of tricalcium phosphate (TCP) polymorphs. *Journal of the European Ceramic Society*, **39**, 3257–3263.
- Suguna K. & Sekar C. (2011) Role of strontium on the crystallization of calcium hydrogen phosphate dihydrate (CHPD). *Journal of Minerals & Materials Characterization & Engineering*, **10**, 625–636.
- Tadier S., Bareille R., Siadous R., Marsan O., Charvillat C., Cazalbou S. et al. (2012) Strontium-loaded mineral bone cements as sustained release systems: compositions, release properties, and effects on human osteoprogenitor cells. *Journal of Biomedical Materials Research Part B: Applied Biomaterials*, **100**, 378–390.
- Tamimi F., Sheikh Z. & Barralet J. (2012) Dicalcium phosphate cements: brushite and monetite. *Acta Biomaterialia*, **8**, 474–487.
- Tortet L., Gavarrı J.R. & Nihoul G. (1997) Study of protonic mobility in $\text{CaHPO}_4 \cdot 2\text{H}_2\text{O}$ (brushite) and CaHPO_4 (monetite) by infrared spectroscopy and neutron scattering. *Journal of Solid State Chemistry*, **132**, 6–16.
- Wu J., Ueda K. & Narushima T. (2020) Fabrication of Ag and Ta co-doped amorphous calcium phosphate coating films by radiofrequency magnetron sputtering and their antibacterial activity. *Materials Science and Engineering C*, **109**, 110599.
- Xue Z., Wang Z., Sun A., Huang J., Wu W., Chen M. et al. (2020) Rapid construction of polyetheretherketone (PEEK) biological implants incorporated with brushite ($\text{CaHPO}_4 \cdot 2\text{H}_2\text{O}$) and antibiotics for anti-infection and enhanced osseointegration. *Materials Science and Engineering C*, **111**, 110782.
- Zhuang F.-Q., Tan R.-Q., Shen W.-F., Zhang X.-P., Xu W. & Song W.-J. (2015) Synthesis of β -type strontium hydrogen phosphate nanosheets and its immobilization of Pb^{2+} in acidic aqueous solution. *Acta Metallurgica Sinica (English Letters)*, **28**, 438–443.